Compact sources as the origin of the soft γ-ray emission of the Milky Way

F. Lebrun[1,2], R. Terrier[1,2], A. Bazzano[3], G. Bélanger[1], A. Bird[4], L. Bouchet[5], A. Dean[4], M. Del Santo[3], A. Goldwurm[1], N. Lund[6], H. Morand[1], A. Parmar[7], J. Paul[1,2], J.-P. Roques[5], V. Schönfelder[8], A. W. Strong[8], P. Ubertini[3], R. Walter[9] & C. Winkler[7]

[1]CEA-Saclay, DAPNIA/Service d'Astrophysique, F91191 Gif sur Yvette Cedex, France
[2]Fédération de Recherche APC, Collège de France, 11, place Marcelin Berthelot, F75231 Paris, France
[3]IASF/CNR, Via del fosso del cavaliere 100, 00133 Roma, Italy
[4]School of Physics and Astronomy, University of Southampton, Highfield, Southampton S017 1BJ, UK
[5]CESR, 9 avenue du colonel Roche – BP 4346, 31028 Toulouse Cedex 4, France
[6]DSRI, Julian Maries Vej 30, DK-2100 Copenhagen 0, Denmark
[7]ESA, RSSD, Keplerlaan 1, NL-2201 AZ Noordwijk, The Netherlands
[8]MPE, Giessenbachstrasse, 85748 Garching bei Munchen, Germany
[9]ISDC, Chemin d'Ecogia, CH-1290 Versoix, Switzerland

The Milky Way is known to be an abundant source of γ-ray photons[1], now determined to be mainly diffuse in nature and resulting from interstellar processes[2]. In the soft γ-ray domain, point sources are expected to dominate, but the lack of sensitive high-resolution observations did not allow for a clear estimate of the contribution from such sources[3,4]. Even the best imaging experiment[5] revealed only a few point sources, accounting for about 50% of the total Galactic flux[6]. Theoretical studies were unable to explain the remaining intense diffuse emission[7,8].

Investigating the origin of the soft γ-rays is therefore necessary to determine the dominant particle acceleration processes and to gain insights into the physical and chemical equilibrium of the interstellar medium[7]. Here we report observations in the soft γ-ray domain that reveal numerous compact sources. We show that these sources account for the entirety of the Milky Way's emission in soft γ-rays, leaving at most a minor role for diffuse processes.

There are two main processes that can lead to an interstellar soft γ-ray emission. The first and the most natural is inverse Compton scattering of high-energy (GeV) cosmic-ray electrons on the ambient photon field. However, the electrons required to account for the bulk of the Galactic emission would also produce radio-synchrotron emission in the Galactic magnetic field at a level much higher than the one actually observed[9]. The second assumes the presence of a population of electrons of a few hundred keV radiating through bremsstrahlung interactions with the interstellar gas. Because these electrons would lose their energy primarily through ionization and Coulomb collisions, the total power required to compensate for their energy losses is of the order of 10^{41}–10^{43} erg s^{-1} (ref. 10). This power, comparable or higher than that of the cosmic ray protons, would affect the interstellar-medium ionization equilibrium and give rise to an excessive dissociation of the interstellar molecules. In the light of the above arguments outlining the improbability of an interstellar origin for the galactic soft γ-ray emission, and taking into account the spectral shape of this emission, the hypothesis of a major point-source contribution was put forth[10,11].

The INTEGRAL γ-ray observatory[12], launched in October 2002, carries two major co-aligned coded-mask instruments: the IBIS imager[13] and the SPI spectrometer[14]. To lessen the instrumental
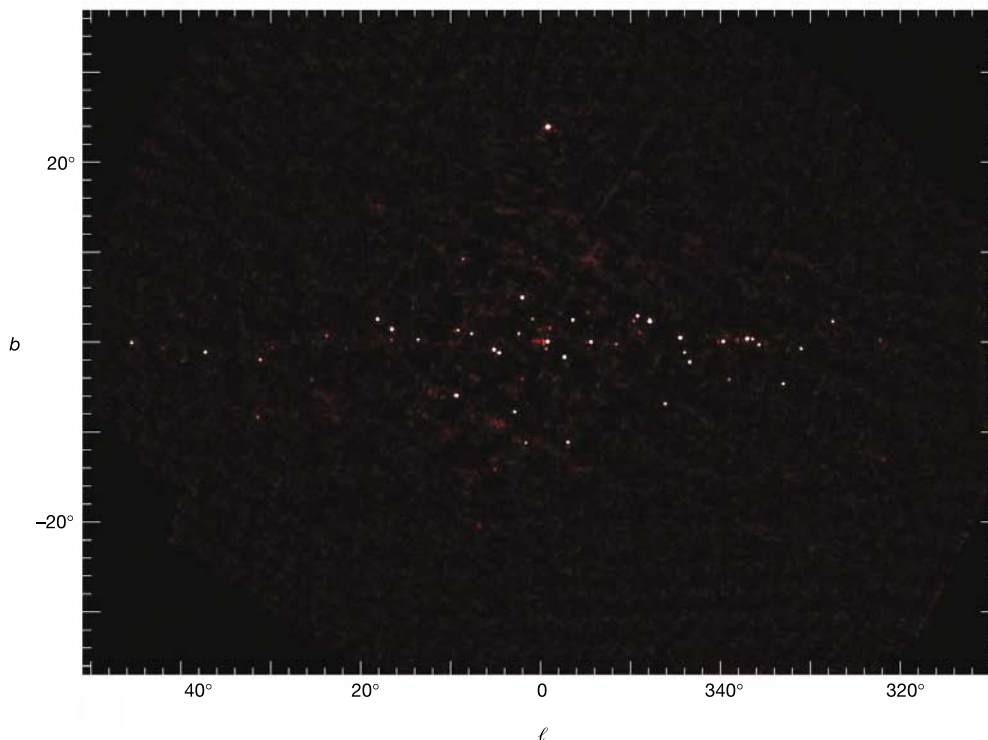

Figure 1 IBIS/ISGRI view of the Galactic Centre region. ISGRI galactic map of the central part of the Milky Way in the 20–60 keV energy band. Most of the 91 sources detected in this image lay in the Galactic plane. The Galactic bulge, the region around the Galactic Centre ($\ell = 0°$, $b = 0°$), is densely populated, especially with low-mass X-ray binaries. This map is a mosaic of about 2,000 images resulting from the IBIS standard analysis[16] of 2.2-ks pointed observations. The standard analysis deconvolves detector images with the mask pattern, detects the significant peaks and subtracts the point spread function (PSF) side-lobes in the resulting sky images. ISGRI[15], the low-energy camera of IBIS, uses 16,384 independent CdTe detectors operating between 15 keV and 1 MeV. With the IBIS mask 3.2 m above, it provides a 13′ angular resolution over a 19° × 19° FWHM field of view and has a sensitivity close to 1 mCrab below 100 keV for a 10^6-s observation. The average point-source location accuracy is a few arcmin[20].

293

background contribution, both experiments are actively shielded. Coded mask imaging acts as a high-pass spatial-frequency filter, strongly attenuating structures larger than the instrument's angular resolution, which is $13'$ for IBIS and $2.6°$ for SPI. This makes IBIS, with its ISGRI[15] photon-counting γ-camera, very well suited to measure the emission from compact sources. Below 100 keV, the IBIS/ISGRI sensitivity reaches the millicrab level.

INTEGRAL observed the Galactic Centre region in the spring and fall of 2003 as part of its core programme (guaranteed time) and during two target-of-opportunity observations. The total observing time amounts to about 1.5×10^6 s in the central part of the survey. Figure 1 shows an IBIS/ISGRI mosaic image produced using the standard analysis software[16]. Sources were detected and removed one by one from the most to the least significant, yielding a list of 91 excesses above 6 sigma. Catalogued counterparts were searched for each of these sources using SIMBAD at the Centre des Données Stellaires de Strasbourg. All but 26 were identified with known sources. Forty of the identified sources are accreting binary systems with low-mass companions as expected in a region that is rich in old stars such as the Galactic bulge.

The remaining sources of known type are: seven high-mass systems, two radio pulsars, two plerionic supernova remnants, one millisecond pulsar, one soft γ-ray repeater and one Seyfert 1 galaxy. This leaves 11 sources of unknown type. The known binaries contribute to the total source flux at levels of 86%, 78%, 77% and 74% respectively in the 20–40, 40–60, 60–120 and 120–220 keV bands. The global spectrum of the other sources is thus significantly harder, possibly indicating a new emerging population of hard sources. Some of the unidentified sources are highly absorbed such as IGRJ16318−4848 (ref. 17), discovered during the course of this survey. A significant contribution from plerions and pulsars could also be considered, as their spectra are much harder than the average.

Diffuse emission is washed out during the standard imaging process, so its contribution can be estimated by comparing the data before and after this processing. This entails comparing the ISGRI count rate and the combined intensity of detected sources. The count rate is due to the internal background, the cosmic diffuse background, the galactic diffuse emission and point sources. If the ISGRI count rates can be corrected for the internal background variations and the contribution from the known point sources removed, we should be left with a Galactic emission, possibly diffuse, and an isotropic contribution; the latter composed of the cosmic diffuse background and the constant internal background.

The internal background has a hard spectrum and fully dominates the count rates above 500 keV. We can therefore use the high-energy ISGRI count-rate to predict the variable part of the internal background. The relation between the count rate in each energy range and that above 500 keV can be derived from high-latitude observations devoid of galactic emission. The variable part of the internal background has been subtracted from each observation window to produce corrected count rates. The contribution of each detected source was computed by applying the IBIS angular response to the intensity at the source position in the field of view. To convert intensities to source count rates, a conversion factor was derived from Crab nebula observations.

Galactic maps of the difference between the corrected and the source count rates were built. Each sky bin was assigned the average of the count rates of all observations pointing within it. The resulting map has a resolution of the order of the field of view (19° full-width at half-maximum, FWHM). These residuals contain an isotropic emission and a Galactic contribution. Their respective importance was fitted to the latitude profile of the residuals. The fitted count rate of this residual Galactic emission is $8.6 \pm 3.0\,\mathrm{s}^{-1}$, $0.2 \pm 1.1\,\mathrm{s}^{-1}$, $0.7 \pm 1.3\,\mathrm{s}^{-1}$, and $-0.7 \pm 0.6\,\mathrm{s}^{-1}$, respectively in the 20–40, 40–60, 60–120 and 120–220 keV bands. A Galactic diffuse
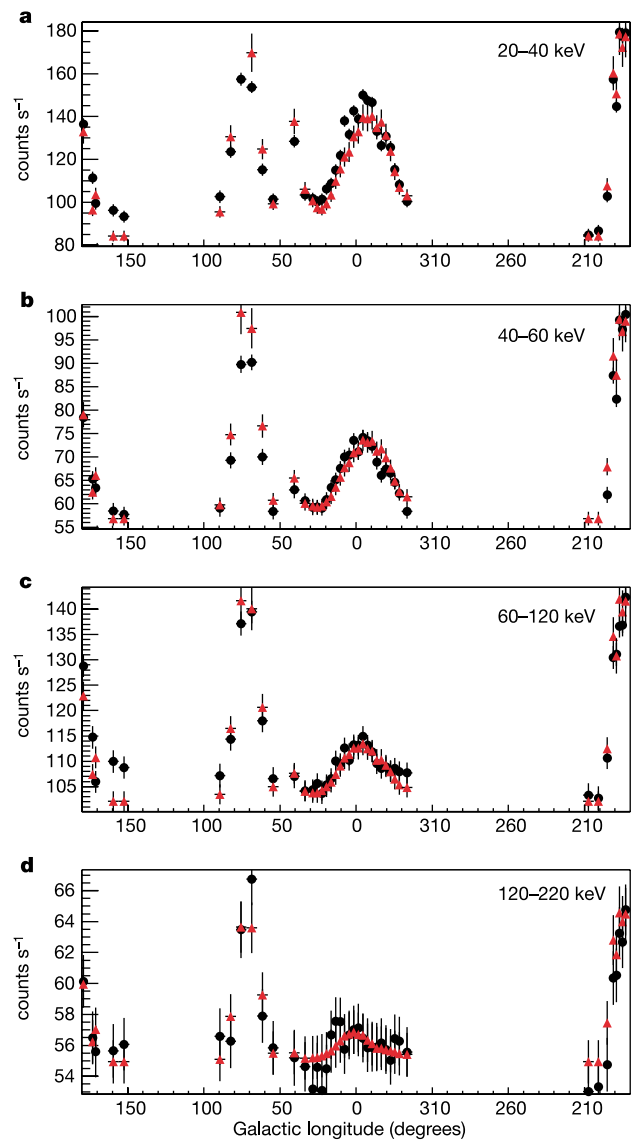

Figure 2 Longitude profile of the Galactic emission at $|b| < 5°$. Comparison between the background-corrected detector count rate (black circles) and the estimated count rate from the detected sources (red triangles) as a function of longitude for each energy band (**a**–**d**). These profiles were produced averaging the corrected count rates of all pointings lying in the same longitude bin, with $|b| < 5°$. The resulting angular resolution is then given by the instrument's field of view. Because the variable internal background dominates all other components above 500 keV, the count rate above that energy can be used to predict and subtract the internal background in each energy range. This correction has been calibrated using the relation between the count rates in each energy range and in the range above 500 keV during high-latitude observations (pointing at $|b| > 30°$) that are deprived of Galactic and point-source emission. The contribution of the Galactic emission above 500 keV does not significantly bias the background subtraction. Even if the total Galactic flux above 500 keV were at the Crab nebula level, the bias introduced in the correction would never exceed $0.3\,\mathrm{s}^{-1}$, which is negligible, at least below 120 keV. The total point-source count rate profile is estimated for each pointing correcting for acceptance and attenuation effects due to the source position in the field of view. The flux obtained through the imagery is then calibrated on the background-corrected crab count rate. The error bars are due to the systematic uncertainties introduced during this process. The constant isotropic background obtained by fitting the latitude distribution (see Fig. 3) has been added to the source count rate.
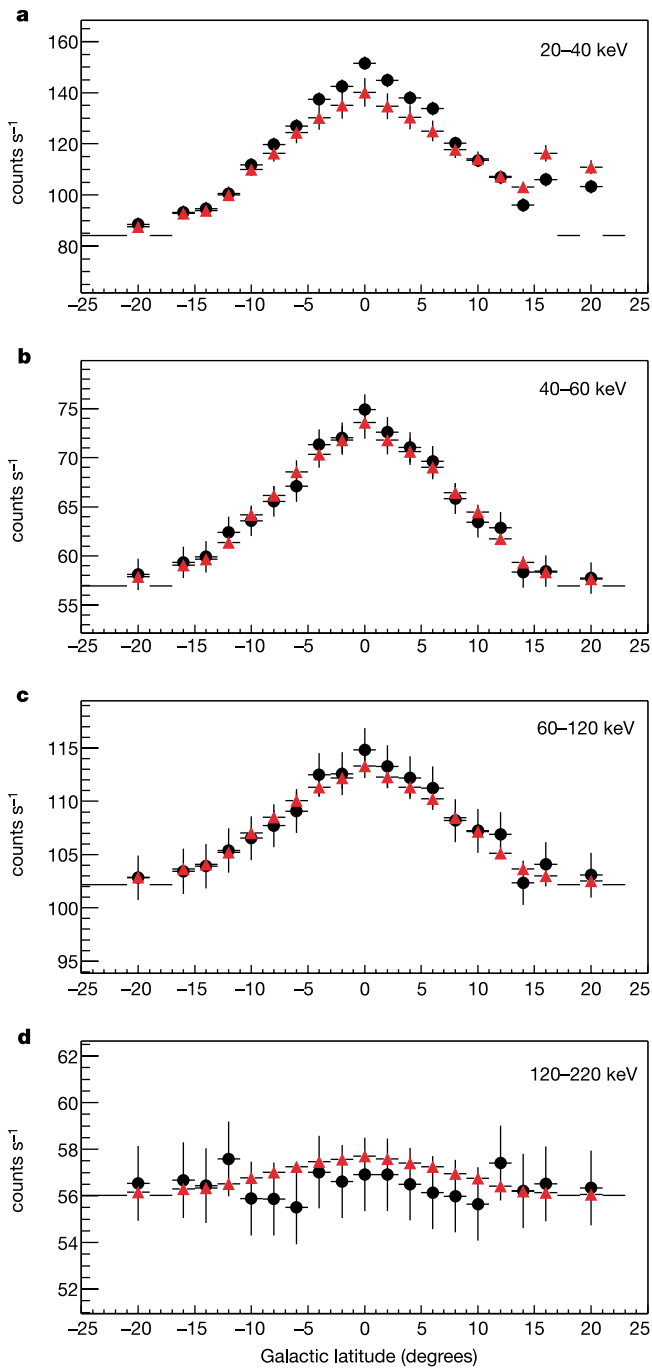
Figure 3 Latitude profiles of the Galactic emission in the central regions where $|\ell| < 20°$. These profiles (**a**–**d**) have been produced as for Fig. 2. They show background-corrected count rates (black circles), and source contribution (red triangles), in the Galactic central regions. The interstellar emission is believed to be distributed as a 5° FWHM gaussian along the Galactic plane[3]. Such a gaussian has been convolved with the IBIS field of view and the resulting Galactic distribution has a width of around 15°. To estimate the amount of residual emission compatible with Galactic emission, we fitted the latitude profile of the difference between corrected count rate and source count rate, with the previously defined Galactic distribution and an isotropic component. The latter have been added to the source count rate in each profile to see the amount of residual emission. A contribution of 13% is visible under 40 keV (**a**). Scorpio X-1 ($b \approx 20°$) is not well accounted for because of the inaccuracies of the response model at large angles. No significant emission is seen at higher energies. In the 120–220 keV band, the systematic errors due to the background subtraction and the source count rate normalization limit the significance of the result.

component contribution of 13% of the total Galactic emission appears below 40 keV. There is no indication of an interstellar emission beyond. We note, however, that at high energy ($>$120 keV) the uncertainty becomes large compared to the total source contribution.

Figure 2 displays the longitude profile of the corrected count rate together with that from the detected sources. The Crab nebula and the equally bright accreting black hole Cygnus X-1 dominate the longitude profiles. At low energy, the Galactic Centre is not much less significant but weakens faster with energy. Although the general agreement between both profiles is very good, particularly at low energies, we notice significant discrepancies. Because our source list is complete only over the central Galactic radian, some of these discrepancies may be due to missing sources. Other discrepancies may be ascribed to inaccurate or inappropriate response functions. In particular, above ~100 keV, the passive shield is no longer fully opaque, although we assumed it was in our computation of the source contribution. Latitude profiles of the corrected count rates are given in Fig. 3. The diffuse Galactic contribution at the 13% level revealed in the fitting procedure is clearly apparent on the top profile. This emission could be due to weaker sources and/or interstellar emission. It is peaked both in latitude and longitude and its ~10° radius is reminiscent of the Galactic bulge strongly populated with low-mass X-ray binaries. At high energy ($E > 120$ keV), the large systematic uncertainties reflect the limitations of the method. It is assumed that the corrected count rates are only due to emission within the field of view but the passive shield is no longer opaque at these energies.

In this regard, we note that SPI, using a large anticoincidence system, is much better shielded at high energy. Strong *et al.*[18] have made a preliminary attempt to estimate the Galactic diffuse emission, separating only the four brightest sources near the Galactic Centre. We wondered what would have been the effect of the 43 sources detected in the simultaneous ISGRI data. Taking advantage of the summed spectra of the four sources measured by both instruments, a cross-calibration can be extracted. The total Galactic emission measured by SPI can be obtained by summing the 'diffuse' and source spectra given in Fig. 2 of ref. 19. The sources detected in the ISGRI data contribute to 86% of the Galactic emission observed with SPI between 100 and 200 keV, giving a heuristic estimate of the source contribution in this energy range.

It appears that the Galactic soft γ-ray emission is fully dominated by compact sources even if a little room still exists for interstellar emission. The difference with the X-ray domain ($<$10 keV) is particularly remarkable[19]. It seems that between 10 and 20 keV a complete change in the mechanisms at the origin of the Galactic emission must occur. However, we should bear in mind the vast difference in spatial resolution between the X-ray and γ-ray experiments. A feature a few arcmin wide will appear as diffuse to Chandra and as a point source to IBIS. Below 40 keV the remaining 13% not accounted for by the detected compact sources could be due to weak bulge sources or to the same mechanism at work below 10 keV. Interstellar processes can still contribute to the soft γ-ray emission of the Galaxy but at such a low level or in so restricted areas that the power supply, ionization or molecule dissociation problems are alleviated.   □

1. Schönfelder, V. *The Universe in Gamma Rays* (A&A Library, Springer, 2001).
2. Strong, A. W., Moskalenko, I. V. & Reimer, O. Diffuse continuum gamma rays from the Galaxy. *Astrophys. J.* **537,** 763–784 (2000).
3. Kinzer, R. L., Purcell, W. R. & Kurfess, J. D. Gamma-ray emission from the inner Galactic ridge. *Astrophys. J.* **515,** 215–225 (1999).
4. Valinia, A., Kinzer, R. L. & Marshall, F. E. Measurement of the Galactic X-ray/gamma-ray background radiation: contribution of point sources. *Astrophys. J.* **534,** 277–282 (2000).
5. Paul, J. *et al.* SIGMA: the hard X-ray and soft gamma-ray telescope on board the GRANAT space observatory. *Adv. Space Res.* **11,** (8)289–(8)302 (1991).
6. Purcell, W. R. *et al.* Diffuse galactic gamma-ray continuum. *Astron. Astrophys. Suppl. Ser.* **120,** 389–392 (1996).

7. Pohl, M. Limits for an inverse bremsstrahlung origin of the diffuse Galactic soft gamma-ray emission. *Astron. Astrophys.* **339,** 587–590 (1998).

8. Dogiel, V. A., Inoue, H., Schönfelder, V. & Strong, A. W. The origin of diffuse X-ray emission from the Galactic ridge. I. Energy output of particle sources. *Astrophys. J.* **581,** 1061–1070 (2002).

9. Webber, W. R. in *Composition and Origin of Cosmic Rays* (ed. Shapiro, M. M.) 83–100 (Boston, Dordrecht, 1983).

10. Skibo, J. G., Ramaty, R. & Purcell, W. R. Implications of the diffuse Galactic continuum. *Astron. Astrophys. Suppl. Ser.* **120,** 403–406 (1996).

11. Lebrun, F. *et al.* Nature of the Galactic soft gamma-ray emission. *Astrophys. Lett. Commun.* **38,** 457–460 (1999).

12. Winkler, C. *et al.* The INTEGRAL mission. *Astron. Astrophys.* **411,** L1–L6 (2003).

13. Ubertini, P. *et al.* IBIS: the imager on-board INTEGRAL. *Astron. Astrophys.* **411,** L131–L139 (2003).

14. Vedrenne, G. *et al.* The spectrometer aboard INTEGRAL. *Astron. Astrophys.* **411,** L63–L70 (2003).

15. Lebrun, F. *et al.* ISGRI: the INTEGRAL Soft Gamma-Ray Imager. *Astron. Astrophys.* **411,** L141–L148 (2003).

16. Goldwurm, A. *et al.* The INTEGRAL/IBIS scientific data analysis. *Astron. Astrophys.* **411,** L223–L229 (2003).

17. Walter, R. *et al.* INTEGRAL discovery of a bright highly obscured galactic X-ray binary source IGR J16318−4848. *Astron. Astrophys.* **411,** L427–L432 (2003).

18. Strong, A. W. *et al.* Diffuse continuum emission from the inner Galaxy: first results from INTEGRAL/SPI. *Astron. Astrophys.* **411,** L447–L450 (2003).

19. Wang, Q. D., Gotthelf, E. V. & Lang, C. C. A faint discrete source origin for the highly ionized iron emission from the Galactic centre region. *Nature* **415,** 148–150 (2002).

20. Gros, A. *et al.* The INTEGRAL IBIS/ISGRI point spread function and source location accuracy. *Astron. Astrophys.* **411,** L179–L183 (2003).

Competing interests statement The authors declare that they have no competing financial interests.

Correspondence and requests for materials should be addressed to F.L. (flebrun@cea.fr).

....

Structural relaxation in supercooled water by time-resolved spectroscopy

Renato Torre[1,2,3]**, Paolo Bartolini**[1,2] **& Roberto Righini**[1,2,4]

[1]*European Laboratory for Non-linear Spectroscopy,* [2]*Instituto Nazionale per la Fisica della Materia,* [3]*Dipartimento di Fisica, and* [4]*Dipartimento di Chimica, Università di Firenze, Polo Scientifico, Sesto Fiorentino, Firenze, 50019 Italia*

....

Water has many kinetic and thermodynamic properties that exhibit an anomalous dependence on temperature[1–5]**, in particular in the supercooled phase. These anomalies have long been interpreted in terms of underlying structural causes, and their experimental characterization points to the existence of a singularity at a temperature of about 225 K. Further insights into the nature and origin of this singularity might be gained by completely characterizing the structural relaxation in supercooled water**[6]**. But until now, such a characterization has only been realized in simulations**[7–9]** that agree with the predictions of simple mode-coupling theory**[10]**; unambiguous experimental support for this surprising conclusion is, however, not yet available**[11–14]**. Here we report time-resolved optical Kerr effect measurements**[15]** that unambiguously demonstrate that the structural relaxation of liquid and weakly supercooled water follows the behaviour predicted by simple mode-coupling theory. Our findings thus support the interpretation**[7–9]** of the singularity as a purely dynamical transition. That is, the anomalous behaviour of weakly supercooled water can be explained using a fully dynamic model and without needing to invoke a thermodynamic origin. In this regard, water behaves like many other, normal molecular liquids that are fragile glass-formers.**

The shear viscosity, self-diffusion coefficient and relaxation times of water above melting and in the supercooled state all exhibit a temperature dependence following a diverging power law[1–5] of the type $(T/T_S - 1)^{-x}$, independent of the measurement method used. Thermodynamic properties such as heat capacity, compressibility and thermal expansion coefficient similarly show a temperature dependence characterized by an anomalous increase upon cooling. Different experimental determinations of the singularity temperature T_S converge on values of about 223–228 K. Although the nature and physical origin of this singularity are still debated[16–18], the observed anomalous phenomena suggest that modifications of structural properties of water occur around this temperature. Characterizing the correlation functions of water and their time evolution, at temperatures below melting and approaching T_S, might therefore yield new insights. But although simulation results suggest that the features of the investigated dynamic correlation functions agree well with the predictions of mode-coupling theory[7–9], unambiguous experimental support for this surprising conclusion is not yet available[11–14].

Several recent time-resolved optical Kerr effect (OKE) experiments on water have revealed[11,19–23] an oscillation on short time-scales (for delay time shorter than 1 ps) in the time profile of the measured signal; at longer times, the signal shows a monotonous
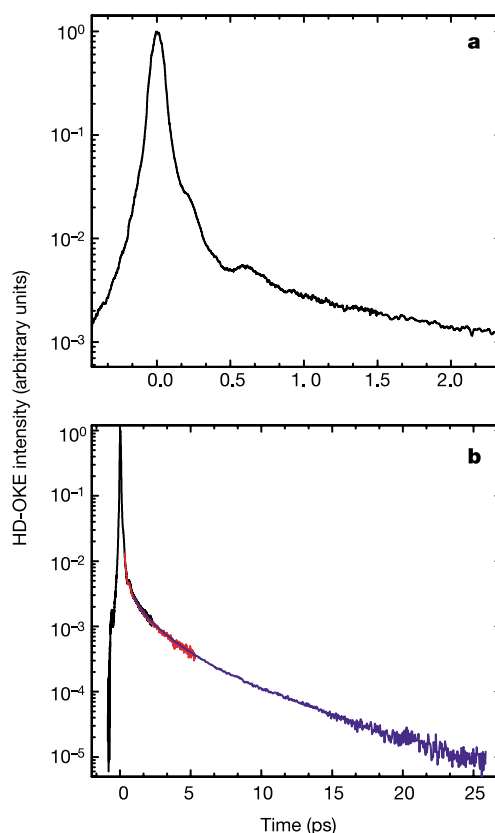

Figure 1 Signal decay measured in the time-resolved HD-OKE experiment on supercooled water at $T = 257$ K. **a**, HD-OKE signal in the short time region. An oscillatory component occurs in the decay trace for time shorter than 1 ps. **b**, HD-OKE signal over the whole time region measured. For longer time the relaxation shows a monotonous decay. The plot illustrates the procedure used for improving the sensitivity. The entire time decay scan was divided into three sections. Short laser pulses (60 fs) were used for the short time scan (black line); for the intermediate time delay intervals (red line) the laser pulse duration was stretched up to 120 fs; for the longer time (blue line) we used stretched laser pulses of 500 fs duration. In this procedure we increased the pulse energy to keep the peak power roughly constant. Care was taken to ensure a large time overlap between subsequent scans, to allow an accurate rescaling of the intensities and a proper reconstruction of the entire decay curve.